Investigation of the Structural and Electrochemical Properties of Size-Controlled SnO_2 Nanoparticles

Hyo-Jin Ahn,[†] Hyun-Chul Choi,[‡] Kyung-Won Park,[†] Seung-Bin Kim,[‡] and Yung-Eun Sung*,[†]

Department of Materials Science & Engineering and Research Center for Energy Conversion and Storage, Kwangju Institute of Science & Technology (K-JIST), Kwangju 500-712, Republic of Korea, and Department of Chemistry, Pohang University of Science and Technology (POSTECH), San 31, Hyojadong, Namgu, Pohang 790-784, Republic of Korea

Received: June 23, 2003; In Final Form: December 1, 2003

Four types of size-controlled SnO_2 nanoparticles were synthesized by a colloidal method to investigate the structural and electrochemical properties of various particle sizes. The samples were characterized by means of transmission electron microscopy (TEM), powder X-ray diffraction (XRD), X-ray photoelectron spectroscopy (XPS), near-edge X-ray absorption fine structure (NEXAFS), and electrochemical measurements. TEM and XRD analyses showed that the samples were well dispersed with an average particle size of ∼20 nm (sample A), ∼11 nm (sample B), ∼5.6 nm (sample C), and ∼2.3 nm (sample D). XPS analyses of four size-controlled SnO_2 samples confirmed that the chemical state of the Sn was Sn^{4+}, as evidenced by the presence of SnO_2, not Sn^{2+} related to the $Sn(OH)_2$. The Sn NEXAFS spectra of the four samples indicated that the samples had a tetragonal rutile structure and showed no noticeable change in the oxidation state of tin ions with decreased particle size, in good agreement with the XPS analysis. The electrochemical properties of lithium insertion in the first cycle were different and systematically varied with a plateau at about 0.8 V in the four types of samples. Furthermore, the optimum particle size for enhanced lithium insertion/extraction was found to be in the range ∼11 nm, among the four types of size-controlled SnO_2 nanoparticles. When the particle size decreased from 11 nm to 5.6 and 2.3 nm, performance inversely decreased due to the absence (or small amounts) of Li_2O phase.

Introduction

Nanometer-sized materials have recently attracted a considerable amount of attention due to their unique electrical, physical, chemical, and magnetic properties as well as their potential for technological applications.[1−4] Although many types of nanoparticles have been shown to exhibit size-dependent physical properties, a number of questions concerning the correlation of the size and physical properties remain unanswered. In particular, factors that determine the critical size at which the properties of a material deviate from those of the bulk material are not well understood.

Nanometer-sized materials in electrode materials may allow the optimum transport of both electrons from the back contact to the front of the electrode and ions from the electrolyte to the electrode particles, which can lead to a rapid discharging and charging rate in a battery.[5] For example, Martin et al. successfully demonstrated the advantage of nanometer-sized host materials for lithium insertion as an anode material for secondary lithium batteries.[6] They proposed that the improved rate and cycling performance are related to the small domain size of the Sn grains within the SnO_2 nanofibers. However, an investigation of the relationship between the size and electronic properties of metal oxide nanoparticles in a battery system is not yet understood and further work is required.

Tin oxide (SnO_2) is an n-type semiconductor that is widely used in a broad range of technical areas as gas sensors, catalysts, battery technology, and transparent electrodes.[7−11] For applications of electrode materials, SnO_2 has been proposed as a possible anode material for replacing the current carbon-based materials because it has higher theoretical capacity (1491 mA h/g).[8] According to previously reported studies,[12,13] the reaction mechanism of SnO_2 with lithium can be summarized by two steps:

$$SnO_2 + 4Li^+ + 4e^- \rightarrow Sn + 2Li_2O \qquad (1)$$

$$Li+ + xe^- + Sn \rightleftharpoons Li_xSn \qquad 0 \le x \le 4.4 \qquad (2)$$

In the first step, Li-inserted SnO_2 forms amorphous Li_2O and metallic Sn. Further reaction of the newly formed metallic Sn with lithium subsequently leads to the formation of Li−Sn alloys with the composition, $Li_{4.4}Sn$. However, the alloying of lithium into bulk metallic Sn causes internal damage due to the large volume expansion, resulting in a loss of capacity and rechargeability. It has recently been pointed out that an electrode composed of nanostructured tin-based materials can deliver a very high capacity (∼700 mA h/g at the 8 C rate) and still retain the ability to be discharged and charged for 800 cycles.[7] This finding has led to a renewed interest in the use of SnO_2 nanoparticles as promising anode materials for use in rechargeable lithium batteries. The critical size of electrochemical properties under 20 nm is an important question that is not well understood at this time. The main objective of this study was

* To whom correspondence should be addressed. Current address: School of Chemical Engineering, Seoul National University, Seoul 151-744, Republic of Korea. E-mail: ysung@ac.kr.
[†] K-JIST.
[‡] POSTECH.

10.1021/jp035769n CCC: $27.50
Published on Web 06/22/2004

to investigate the effect of particle size on the structural and electrochemical properties of SnO_2 nanoparticles.

Experimental Section

Four types of size-selected SnO_2 nanoparticles were prepared by a colloidal method in an aqueous solution under an ambient atmosphere. $SnCl_4 \cdot 5H_2O$ (99%), Na_2CO_3 (99%), or $NaSO_3$ (99%) was used as starting material. Tin salt (0.5 g) was dissolved in 300 mL of deionized water with stirring, and then 5 mL of hydrogen peroxide was added. The pH of the solution was adjusted to 6 with a 0.05 M KOH solution, to avoid the irreversible reaction. Four types of size-controlled SnO_2 particles were subsequently obtained by freeze-drying at −50 °C (sample D) and heat treatment at 380 °C (sample C), 500 °C (sample B), and 700 °C (sample A), respectively.

Structural analyses of the SnO_2 were carried out by transmission electron microscopy (TEM) and X-ray diffraction (XRD). TEM images were obtained as a bright field image and examined by transmission electron diffraction (TED), magnified by 1 100 000 and viewed on a Phillips CM20T/STEM electron microscope at an accelerating voltage of 200 kV. Each sample of the four size-controlled SnO_2 nanoparticles in ethanol was placed on a TEM grid, and the grid was then allowed to dry in a vacuum oven. XRD (Rigaku X-ray diffractometer equipped with a Cu Kα source) analysis of the as-prepared nanoparticles was used to determine the structure and degree of crystallinity. Data were collected over the range of 20°−65° in increments of 0.05° at room temperature. XPS analyses were performed using a VG Scientific (ESCALAB 250) photoelectron spectrometer. The X-ray source was Al Kα with 1486.6 eV operating at 15 kV and 150 W. Samples were prepared by depositing the catalyst on a Cu double-sided tape (3M Inc.). The base pressure of the system was 2×10^{-9} Torr. The Sn M-edge near-edge X-ray absorption fine structure (NEXAFS) measurements of SnO_2 nanoparticles were performed at the U7 beam line of a Pohang Light Source (PLS). Details of the design of the monochromator and the spectral resolution of the beam line are given elsewhere.[14,15] The Sn M-edge NEXAFS data were taken in a total electron yield mode, recording the sample current. The energy resolution was less than 0.2 eV. All spectra were normalized by a reference signal from an Au mesh with a 90% transmission. The base pressure of the experimental chamber was on the order of 10^{-8} mbar.

The electrochemical behavior of nanosized SnO_2 was investigated in organic electrolyte lithium cells using a WBCS 3000 battery tester system (Won A Tech Corp., Korea). Slurries, consisting of 70 wt % SnO_2 powder, 10 wt % acetylene black, and 20 wt % poly(vinylidene fluoride) (PVDF) were dissolved in *N*-methylpyrrolidinone (NMP). The electrodes were prepared by coating the slurry onto a Cu foil substrate. Test cells were fabricated with these electrodes, metallic lithium anodes, and polypropylene separators in a glovebox filled with Ar gas. A 1.0 M $LiPF_6$ solution in a 1:1 (vol %) mixture of ethylene carbonate (EC) and diethyl carbonate (DEC) was used as the electrolyte. The test cells were aged for 24 h at 25 °C after the addition of the electrolyte before electrochemical testing. Cyclic voltammograms by means of AUTOLAB by Eco Chemie were evaluated in 1.0 M $LiPF_6$ (EC:DEC = 1:1 (vol %)) with a scan rate of 0.5 mV s^{-1} at a cutoff voltage of 0.1−2.0 V vs Li/Li^+.

Results and Discussion

Figure 1 shows TEM images and TED patterns for four samples of size-controlled SnO_2 nanoparticles obtained by the colloidal method. As shown in Figure 1, these samples were well dispersed with an average particle size of ∼20 nm for sample A, ∼11 nm for sample B, ∼5.6 nm for sample C, and ∼2.3 nm for sample D. The crystalline (101) plane of the SnO_2 nanoparticles was readily observed in the high-resolution TEM images, suggesting that the crystallinity of each samples is excellent. The TED patterns show that SnO_2 nanoparticles consist of a polycrystalline structure due to the uniform central and diffraction spots. As the particle size decreased, the diffraction patterns of nanoparticles were gradually transformed from spot patterns (bulk scale) to ring patterns (nano scale). This indicates that accurately defined, size-controlled SnO_2 nanoparticles in the range 2.3−20 nm were grown. To further elucidate the structural properties of the samples, XRD data were collected for four size-controlled samples of SnO_2 nanoparticles.

Figure 2 shows powder XRD patterns for the four samples. The XRD patterns of these samples are in good agreement with that of cassiterite SnO_2 (JCPDS Card No. 41-1445). The XRD results confirm that the size-controlled SnO_2 nanoparticles obtained by the colloidal method are present as cassiterite (SnO_2), which has a tetragonal rutile structure (space group $p4/mnm$) with two SnO_2 formula units per unit cell. As shown in Figure 2, the XRD peaks of these samples become progressively broader when the particle size decreases from 20 to 2.3 nm. That is, the full width at half-maximum (FWHM) of sample D was much broader than those of samples C, B, and A, indicating that the average particle size of sample D was the smallest among samples A, B, and C as shown in Table 1. To investigate the particle sizes, the mean grain size (D) of these samples was calculated by using the Scherrer equation to the (211) plane diffraction peak ($2\theta = 51.7°$):

$$D = 0.9\lambda/(\beta \cos \theta) \tag{3}$$

where λ is the X-ray wavelength, β is the pure full width of the diffraction line at half its maximum intensity, and θ is the Bragg angle. The mean grain sizes of samples A, B, C, and D were ∼20, ∼11, ∼5.6, and ∼2.3 nm, respectively. The particle sizes of these samples, as determined from the XRD results, are in good agreement with the values obtained from the TEM images.

To obtain information relative to the chemical states of the SnO_2 nanoparticles, XPS analysis was performed as shown in Figure 3. The SnO_2 appears as a spin−orbit doublet at ∼486.7 ($3d_{5/2}$) and ∼495.1 eV ($3d_{3/2}$) with an area ratio of 1.5. That the chemical state in the prepared SnO_2 nanoparticles was Sn^{4+}, and not Sn^{2+} in the hydroxide ($Sn(OH)_2$), was confirmed by XPS analysis of four size-controlled SnO_2 samples.[16] To elucidate the structural and electronic properties associated with the decreased particle size, a NEXAFS analysis was carried out on the size-controlled nanoparticles.

Figure 4 shows the Sn M-edge NEXAFS spectra of the four types of SnO_2 nanoparticles compared to those of the reference materials. Because the NEXAFS measurements involve the excitation of electrons from a core level to the partially filled and empty states, the peak positions and spectral features of the NEXAFS spectrum are affected not only by oxidation state but also by other chemical features of Sn species, such as structural symmetry and covalent/ionic character of the bond between Sn and neighboring atoms.[17,18] In comparison to the reference material, the main spectral features of the SnO_2 nanoparticles show no detectable variation when the particle size is decreased from 20 to 5.6 nm. This indicates that the prepared samples have a tetragonal structure, and that no change in the oxidation state of tin ions with decreased particle sizes should be anticipated. However, they show peak broadening and a reduction in intensity with decreasing particle size, and

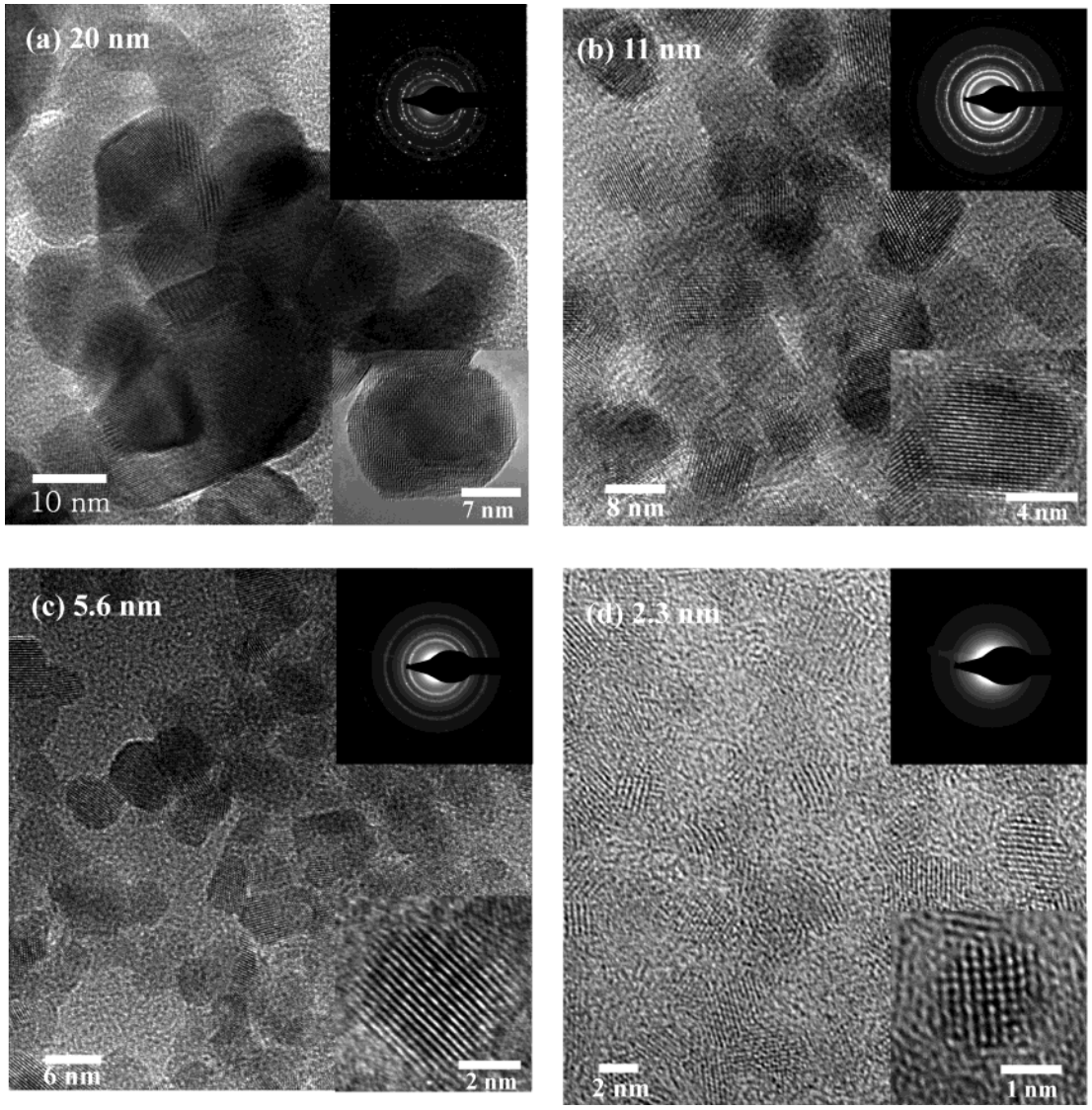

Figure 1. TEM images of (a) sample A, (b) sample B, (c) sample C, and (d) sample D. The inset at the top right of each panel represents the transmission electron diffraction (TED), and the inset at the bottom right corresponds to the (101) plane in a high-resolution TEM (HRTEM) image.

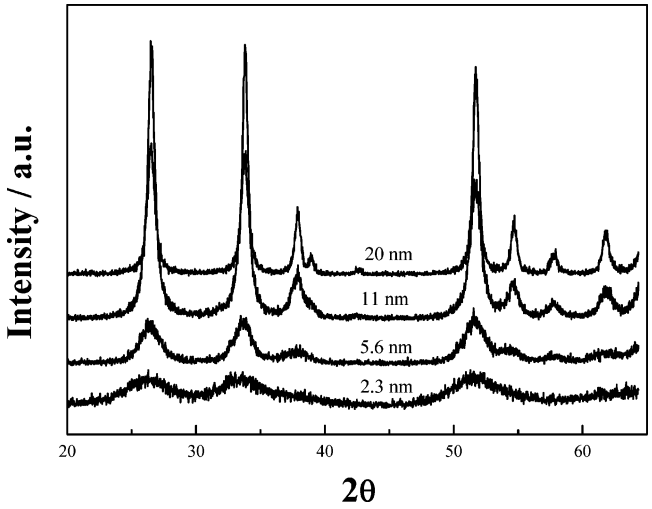

Figure 2. Powder XRD patterns of samples A−D.

sample D with a mean grain size of 2.3 nm shows very weak features. This observation can be attributed to the effect of a smaller particle size. In the X-ray absorption measurements, the probability of exciting an electron is typically described in terms

TABLE 1: Average Particle Sizes, as Determined by XRD of Samples A−D

sample	$2\theta^a$	fwhm[b]	particle size (nm)
A	51.7	0.457	20 ± 2
B	51.7	0.798	11 ± 0.6
C	51.7	1.639	5.6 ± 0.3
D	51.7	3.890	2.3 ± 0.1

[a] In (211) plane. [b] Full width at half-maximum.

of the X-ray absorption cross section.[18] It is proportional to the energy density of the final states and the orientation of the X-ray absorption direction in the coordinate system, which are correlated with the degree of crystallinity of the material. When the particle size decreases to the nanometer scale, no crystal lattice of a long-range order exists in the SnO_2 nanoparticle. Thus, the lack of its long-range order causes a reduction in the intensity of the peaks in the NEXAFS spectra.

Figure 5a shows voltage vs lithium content (x) curves for the Li/SnO_2 cell with size-controlled SnO_2 electrodes at a constant current density of 0.5 mA/cm^2 in the voltage range 0.1−2.0 V. During the first lithium insertion, the potential rapidly drops, reaching a plateau, and then continuously decreases to 0.1 V. One clear difference among the four types of size-controlled SnO_2 electrodes is closely related to the

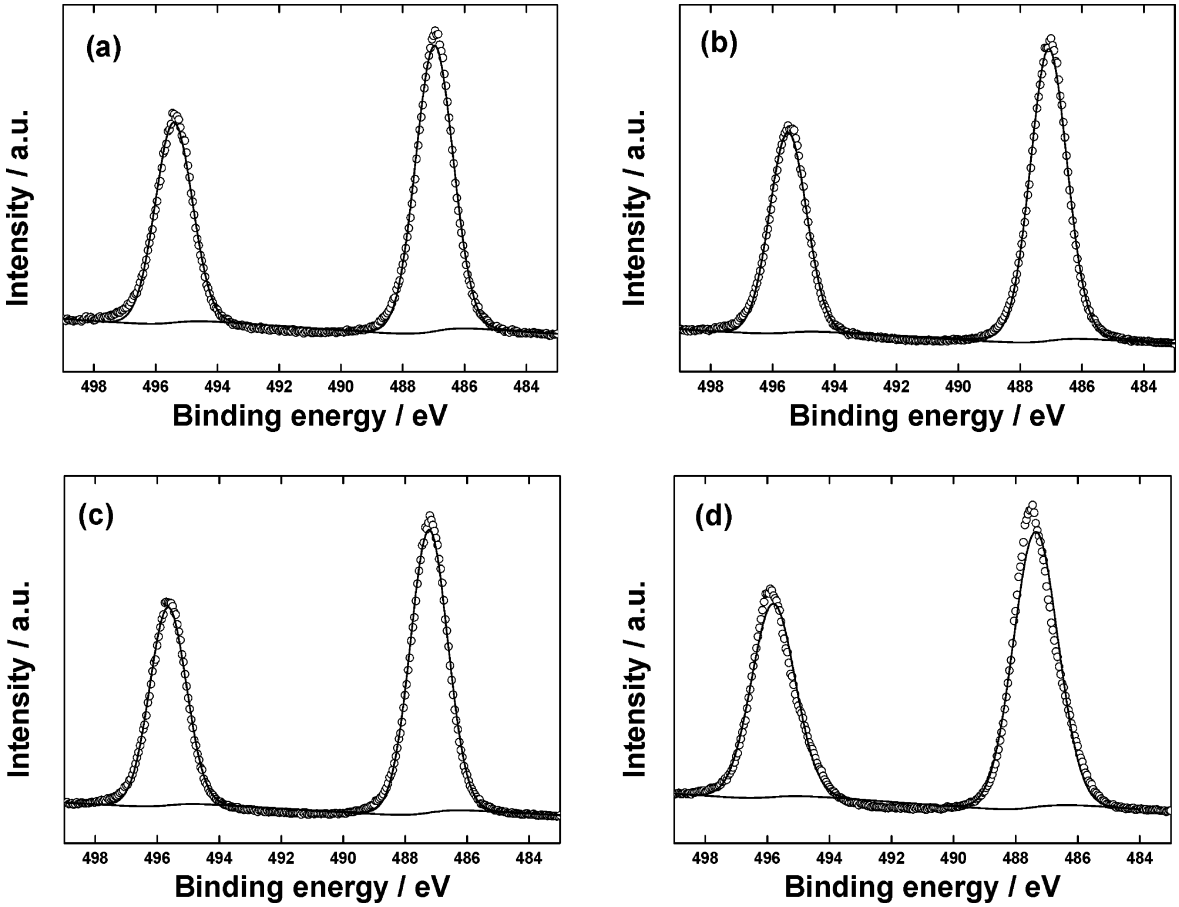

Figure 3. XPS spectra of (a) sample A, (b) sample B, (c) sample C, and (d) sample D.

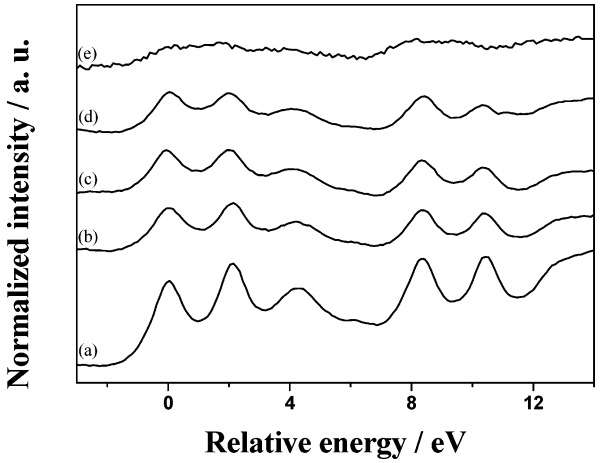

Figure 4. Sn M-edge NEXAFS spectra of (a) reference SnO_2 (Aldrich, 98% 325 mesh), (b) sample A, (c) sample B, (d) sample C, and (e) sample D.

plateau at about 0.8 V due to the formation of a Li_2O phase. Sample A (∼20 nm) and sample B (∼11 nm) in Figure 5a showed classical plateaus around 0.8 V similar to that of a bulk SnO_2 system, which is well-known from previously reported studies.[13,19−22] The Li_2O phase, formed during the first insertion, has been reported to be electrochemically inactive during the subsequent cycles. The Li_2O phase serves as a binding medium that resists the cracking of the electrode induced by the large volumetric change that occurs in Sn−Li alloys during cycling.[23] In our work, when the particle size decreased from 11 to 5.6 nm, the plateau around 0.8 V disappeared, and completely vanished for sample D (∼2.3 nm). Thus, in the case of samples C and D, the mechanism of lithium reactivity appears to be different from the typical lithium insertion/extraction or lithium-alloying process. This result is in good agreement with cyclic voltammograms obtained from conventional three-electrode electrochemical cells, as shown in Figure 5b. As the particle size decreases, the peak at about 0.6 V tends to disappear. These results indicate that Li_2O is formed only in small quantities by reaction 1 as the particles size decreases. This may be related to the enhanced surface electrochemical reactivity due to the much larger surface-to-bulk ratio.[24] At potentials below 0.6 V in Figure 5a, reaction of the newly formed metallic Sn with lithium leads to the formation of Li−Sn alloys which may form a number of Li_xSn as follows:

$$Li^+ + xe^- + Sn \rightleftharpoons Li_xSn \qquad 0 \le x \le 4.4$$

When the particle size decreased from 20 to 2.3 nm, an amount of Li−Sn alloys in the first insertion relatively increases due to the absence of Li_2O. In addition, in the case of bulk-scale tin oxide, it is well-known that the second step of tin oxide follows a reversible process as shown in previous work.[13,19,23] However, it seems that the formation process of Li_xSn in the range of ∼5.6 and ∼2.3 nm is irreversible compared to that of ∼20 and ∼11 nm in the first insertion/extraction process.

Figure 5c shows the optimum particle size for enhanced lithium insertion in the first insertion process. For sample A, SnO_2 reacts with 7.87 lithium atoms per formula unit in the first insertion process, and in the following extraction process about half are removed. Sample B reacts with 8.6 lithium atoms per formula unit and shows a better electrochemical performance than sample A due to the higher utilization of reactive sites as the particle size decreases. However, samples C and D show

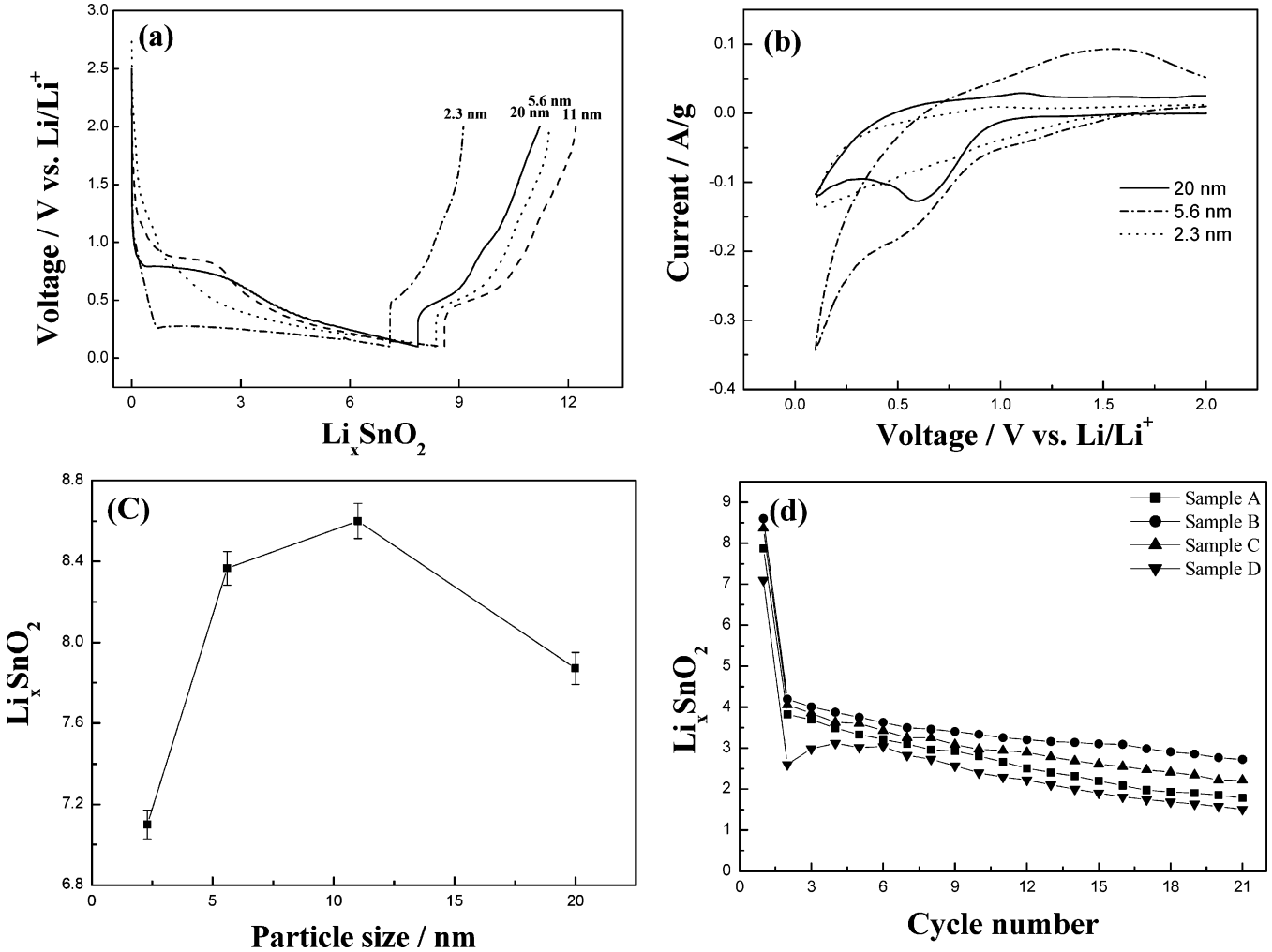

Figure 5. (a) Voltage vs lithium content curves for Li/SnO_2 cells with four types of size-controlled SnO_2 nanoparticles at a constant current density of 0.5 mA/cm^2 at a cutoff voltage of 0.1−2.0 V vs Li/Li$^+$. (b) Cyclic voltammograms of sample A (∼20 nm), sample C (∼5.6 nm), and sample D (∼2.3 nm) fabricated by a colloidal method in 1.0 M $LiPF_6$ (EC:DEC = 1:1 (vol %)) with scan rate of 0.5 mV s^{-1}. (c) Optimum particle size for enhanced lithium insertion for the four types of size-controlled SnO_2 nanoparticles in the first insertion process. (d) Li_xSnO_2 vs cycle number for the same cells under similar conditions for four types of size-controlled SnO_2 nanoparticles, in which the cutoff voltages were 0.1 and 2.0 V.

an inversely decreased performance with 8.36 and 7.1 lithium atoms per formula unit, respectively, despite their decreased sizes. This result may be related to the plateau of Li_2O phase at around 0.8 V in Figure 5a (and Figure 5b), which disappeared. In particular, sample D reacts with 7.1 lithium atoms per formula unit, and upon the subsequent charging process about two-thirds of the lithium is removed. That is, the performance of sample D is inferior to that of the other samples. Despite the smallest particle size, the decreased capacity of sample D may be caused by the absence (or a small amount) of Li_2O phase.[25] Sample D may undergo a larger electrochemical agglomeration due to the absence of a Li_2O phase. Smaller nanoparticles (∼2.3 nm) undergo extensive agglomeration, and their surface energy is substantially decreased. Further, as the size decreases, the growth of the solid−electrolyte interface (SEI) layer would be increased due to its surface area.[26] Once such a serious agglomeration occurs, smaller nanoparticles covered with an SEI film may be embedded within the agglomerated assembly and irreversibly produce extrinsic defects. Once lithium ions are trapped, it may be impossible to extract all of them by the charged mode. A recent study of SnO_2 confirmed that the oxide matrix can restrain the growth of nanosized Li−Sn alloys.[12,27,28] Thus, a suitable inert matrix (a Li_2O phase) is necessary to improve the electrochemical properties of nanosized alloy anodes. Accordingly, the optimum particle size for enhanced lithium insertion/extraction is in the range of ∼11 nm, in which a Li_2O phase was present as shown in Figure 5a.

To further investigate optimum conditions for the various particle sizes, capacity retentions were collected for the four size-controlled nanoparticles, as shown in Figure 5d. Sample B shows a higher performance and good stability, compared to other samples. For the case of sample D, the reversible retention decayed and was unstable due to larger electrochemical agglomeration which is related to the absence of Li_2O phase. Therefore, a highly efficient performance for nanometer-sized materials could be realized by achieving an optimized particle size, thus permitting the preparation of better battery materials. However, since such an optimum particle size can vary with the synthesis method and the type of materials used, the relationship between particle size vs reactivity and the utilization of reactive sites will require further work, which is currently underway. In addition, as the particle size decreases, the growth of SEI layers will appear to become more rapidly detrimental to small particles rather than large ones. If the SEI layer is relatively too large, it will obstruct nanosized SnO_2 reactivity toward lithium. More study will be needed to better understand the effect of the SEI layer.

Conclusion

To elucidate the structural and electrochemical properties of various particle sizes, four types of size-controlled SnO_2 nanoparticles were synthesized by a colloidal method and were analyzed by TEM, XRD, XPS, NEXAFS, and electrochemical measurements. The TEM, XRD, and XPS results showed that the size-controlled SnO_2 nanoparticles were synthesized and had tetragonal rutile structures (cassiterite SnO_2). Further, the NEXAFS spectra showed that peak broadening and a reduction in intensity with four types of size-controlled SnO_2 nanoparticles are closely related to particle size. In the case of electrochemical measurements, it was found that different electrochemical properties associated with lithium insertion in the first cycle markedly varied with the four types of samples, indicating that particle size has a significant influence on the insertion/extraction properties. One clear difference among the four types of nanoparticles was related to the plateau at about 0.8 V due to differences in reaction properties. The optimum particle size for enhanced lithium insertion/extraction was found to be in the range ~11 nm. This may be attributed to the proper formation of a Li_2O phase and a higher utilization of reactive sites on the particles.

Acknowledgment. This work was supported by a grant (code #04K1501-02121) from the Center for Nanostructured Materials Technology under the 21st Century Frontier R&D Program of the Ministry of Science and Technology, KOSEF through the Research Center for Energy Conversion and Storage, and the Brain Korea 21 project from the Ministry of Education.

References and Notes

(1) Weller, H. *Angew. Chem., Int. Ed. Engl.* **1993**, *32*, 41.
(2) Park, K.-W.; Ahn, K.-S.; Choi, J.-H.; Nah, Y.-C.; Kim, Y.-M.; Sung, Y.-E. *Appl. Phys. Lett.* **2002**, *81*, 907.
(3) Buffat, P.; Borel, J. P. *Phys. Rev. A* **2002**, *13*, 2287.
(4) Park, K.-W.; Ahn, K.-S.; Choi, J.-H.; Nah, Y.-C.; Sung, Y.-E. *Appl. Phys. Lett.* **2003**, *82*, 1090.
(5) Attard, G. S.; Elliott, J. M.; Bartlett, P. N.; Whitehead, A.; Owen, J. R. *Macromol. Symp.* **2000**, *156*, 179.
(6) Li, N.; Martin, C. R. *J. Electrochem. Soc*. **2001**, *148*, 164.
(7) Li, N.; Martin, C. R.; Scrosati, B. *Electrochem. Solid-State Lett*. **2000**, *3*, 316.
(8) Aegerter, M. A.; Reich, A.; Ganz, D.; Gasparro, G.; Putz, J.; Krajewski, T. *J. Non-Cryst. Solids* **1997**, *218*, 123.
(9) Idota, Y.; Nishima, M.; Miyaki, Y.; Kubota, T.; Miyasaki, T. *Science* **1997**, *276*, 1395.
(10) Leite, E. R.; Weber, I. T.; Longo, E.; Varela, J. A. *Adv. Mater*. **2000**, *13*, 965.
(11) Spence, W. J. *Appl. Phys*. **1967**, *38*, 3767.
(12) Courtney, I. A.; Dahn, J. R. *J. Electrochem. Soc*. **1997**, *144*, 2045.
(13) Courtney, I. A.; Dahn, J. R. *J. Electrochem. Soc*. **1997**, *144*, 2943.
(14) Lee, M. K.; Shin, H.-J. *Nucl. Instrum. Methods Phys. Rev. A* **2001**, *467*, 508.
(15) Shin, H.-J.; Chung, Y. M.; Kim, B. S. *J. Electron Spectrosc. Relat. Phenom*. **1999**, *101*, 985.
(16) Maciel, A. P.; Lisboa-Filho, P. N.; Leite, E. R.; Paiva-Santos, C. O.; Schreiner, W. H.; Maniette, Y.; Longo. E. *J. Eur. Ceram. Soc*. **2003**, *23*, 707.
(17) Stöhr, J. *NEXAFS Spectroscopy*; Springer-Verlag: New York, 1992.
(18) Chen, J. G. *Surf. Sci. Rep*. **1997**, *30*, 1.
(19) Panero, S.; Savo, G.; Scrosati, B. *Electrochem. Solid-State Lett*. **1999**, *2*, 365.
(20) Grugeon, S.; Laruelle, S.; Herrera-Urbina, R.; Dupont, L.; Poizot, P.; Tarascon, *J. Electrochem. Soc*. **2001**, *148*, 285.
(21) Li, H.; Huang, X.; Chen, L. *Electrochem. Solid-State Lett*. **1998**, *1*, 241.
(22) Retoux, R.; Brousse, T.; Schleich, D. M. *J. Electrochem. Soc*. **1999**, *146*, 2472.
(23) Kim, J. Y.; King, D. E.; Kumta, P. N.; Blomgren, G. E. *J. Electrochem. Soc*. **2000**, *147*, 4411.
(24) Poizot, P.; Laruelle, S.; Grugeon, S.; Dupont, L.; Tarascon, J.-M. *Nature* **2000**, *407*, 495.
(25) Peled, E. *J. Electrochem. Soc*. **1979**, *126*, 2047.
(26) Li, H.; Shi, L.; Wang, Q.; Chen, L.; Huang, X. *Solid State Ionics* **2002**, *148*, 247.
(27) Li, H.; Huang, X.; Chen, L.; Zhou, G.; Zhang, Z.; Yu, D.; Mo, Y. J.; Pei, N. *Solid State Ionics* **2000**, *135*, 181.
(28) Li, H.; Huang, X. J.; Chen, L. Q. *Electrochem. Solid-State Lett*. **1998**, *1*, 244.